

# End-to-end RNA Secondary Structure Prediction using Deep Neural Network

## 1 Introduction

Unlike DNA which typically forms stable double helix between two molecules, RNA is highly flexible so a single RNA molecule can fold onto itself by forming base pairs via hydrogen bond, including Watson-Crick pairs A-U, G-C and non-canonical pairs such as G-U. Base pairs form local structures like stems and loops, which assemble into the global secondary structure.

State-of-the-art RNA secondary structure prediction algorithms like ViennaRNA[1] and Mfold[2] are thermodynamics based. Free energy of each type of local structure is measured experimentally, and total free energy is assumed to be the sum of local terms, which is minimized efficiently via dynamic programming (DP). Although researchers have worked out a large set of local structure types and their associated formulation for free energy calculation, there is no guarantee that it is accurate and complete. There have been effort to fine tune the free energy parameters by training on experimentally solved structures[3], but it is still limited by the known set of local structure types. Another limitation of DP-based approaches is that it is incapable of predicting nested base pairs that appear in structure like pseudoknot.

On the other hand, over the last decade, combination of RNA structure probing and high throughput sequencing has enabled the measurement of genome-wide RNA structural at single nucleotide resolution in multiple organisms and cell types[4, 5]. Due to the level of noise and missing data present in high throughput experiments, we will need a modeling approach that is more flexible and can be trained on different types of data.

In this work, we propose a deep neural network that can be trained end-to-end on sequences and structures. When conditioned on the input RNA sequence, the model can generate a distribution of structures, including ones with pseudoknot.

### 1.1 Problem Formulation

Given a RNA sequence of length  $L$ , we are interested in all possible secondary structures it can take on. For a specific structure, there are three commonly used representations: (1) undirected graph, where each node is a base in the sequence, and each edge represents base pairing. (2) Upper triangular matrix (excluding the diagonal) of size  $L \times L$  with binary values, where a value of 1 at  $(i, j)$  represents base pairing between sequence position  $i$  and  $j$ , and 0 represents no base pairing. (3) Dot-bracket notation of length  $L$  where unpaired bases are denoted as dots, and paired bases are represented as left and right brackets. When pseudoknot is present, different styles of bracket needs to be used to represent nested structures.

As an example, for a short RNA sequence GUUGU-GAAAU, one possible structure it can take on consists of a stem and a loop, as seen in Fig 1(a), represented by an undirected graph. Such structure can also be represented by a  $10 \times 10$  upper triangular matrix with all 0's, except for positions (1, 10), (2, 9) and (3, 8), all being 1, as shown in Fig 1(b). This contiguous stretch of 1's along the diagonal corresponds to the stem formed by the three base pairs: G-U, U-A and U-A. The equivalent dot-bracket notation is shown in Fig 1(c), where the stem is represented by three pairs of left-right brackets.

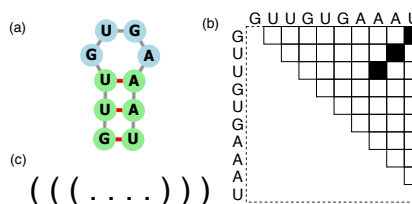


Figure 1: Three different ways to represent secondary structure. (a) undirected graph, generated by [6], (b) upper triangular binary matrix, (c) dot-bracket notation.

### 1.2 Related Work



## 2.1 Model

We propose an architecture that builds global structure from interactions between different positions in the sequence, with neither assumptions on the types of local structures nor hard-coded parameters, such that the entire model can be trained end-to-end using only sequences and structures. The architecture consists of the following components:

1. Two sets of 1D conv layers on the one-hot-encoded sequence are run in parallel, with each set having multiple layers at different resolutions. Activations of the 1D conv layer, one from each set, are used to form a 2D feature map via inner product along the feature dimension, as shown in Fig 3 from (a) to (b). This is inspired by the fact that base pairing is not only affected by the two bases but also surrounding sequences. Such architecture enables the neural network to learn features that affect interaction between any two positions in the sequence.
2. Multiple 2D feature maps, each produced by one pair of 1D activations at a specific layer, are concatenated, as shown in Fig 3 from (b) to (c). This is followed by several 2D conv layers, as shown in Fig 3 from (c) to (d) (showing only one layer for simplicity).
3. Activation of the last 2D conv layer is concatenated with output from the previous "timestamp"  $y^{t-1}$ , and passed through multiple layers of masked 2D conv layers, as shown in Fig 3 from (e) to (f) (showing only one layer for simplicity), which masks "future" (top right) timestamps.
4. Finally, a fully connected layer along the feature dimension with sigmoid activation produces an output between 0 and 1, for each position in the upper triangular matrix, as illustrated in Fig 3 from (f) to (g).

As shown in Fig 3, we refer to 1-2 as the sequence encoder, and 3-4 as the sequence generator.

## 2.2 Training

We trained the model using a synthetic dataset, constructed by sampling 50000 random sequences (each base sampled *i.i.d.* uniformly from  $\{A, C, G, U\}$ ) with length between 10 and 100. For each sequence, we ran RNAfold[1] with default parameters and recorded the minimum free energy structure.

(will table save some space?) The model has 5 pairs of 1D-conv layers, each having 256 filters, with filter width and dilation rate being  $(7, 1), (5, 2), (5, 2), (5, 4), (5, 4)$ . There are 5 masked 2D-conv layers, each having 50 filters, with filter size and dilation rate being  $([3, 3], 1), ([3, 3], 2), ([5, 5], 2), ([9, 9], 4), ([9, 9], 4)$ . Full connected layer has 20 hidden units. All activations are ReLu, except for the output layer being sigmoid. 40000 sequences were used for training and 10000 for validation, with minibatch of 10 sequences. Adam optimizer was used with learning rate 0.001 and the model was trained for 200 epochs with early stopping.

For each minibatch, we zero-pad the sequence array and structure matrix to the maximum length in the minibatch. When computing the loss and gradient, entries in structure matrix that were padded are being masked, in addition to the lower triangular entries, since we're only predicting the upper triangular matrix. At training time, prediction, loss and gradient of all positions in the output are computed in parallel, by passing in the target structure matrix as both the input and target.

## 2.3 Inference

At test time, we sample structures conditioned on the input sequence. As shown in Fig 4, we first pass the sequence through the sequence encoder network to get

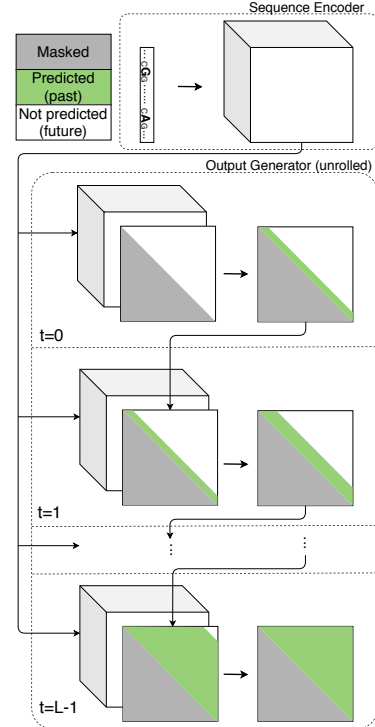


Figure 4: Sample structures conditioned on the input sequence.

the 2D feature map, after that we initialize the structure matrix with all zeros, concatenate it with the 2D feature map, then sample one slice at a time until the upper triangular matrix is filled with sampled values. At each step, we sample a binary label for each position in the current slice based on the Bernoulli probability predicted by the model. To ensure the sampled structure is valid, when sampling the label for location  $(i, j)$ , if  $i$ -th or  $j$ -th position is already paired with another position (from samples in previous timestamps), we set  $y_{i,j}$  to 0 without sampling from the model output. For a sequence of length  $L$ , we run  $L - 1$  steps sequentially.

### 3 Result

#### 3.1 Test set performance

To evaluate the model on unseen data, we generated a test set with 100 sequence, using a process similar to the training set. Sequences are generated with length between 10 and 100. For each sequence in the test set, we ran RNAfold and sampled 100 structures from the ensemble. We also used our model to sample 100 structures from the output distribution conditioned on the input sequence. To avoid evaluating on low probability structures, structures that only occur once were discarded. For each unique structure produced by RNAfold, we computed sensitivity (number of correctly predicted base pairs divided by number of true base pairs) and positive predictive value (PPV, a.k.a. precision, number of correctly predicted base pairs divided by number of predicted base pairs) against all unique structures generated by our model, and recorded the best one, where best is defined by largest sensitivity + PPV. This indicates how well the model recovers each of structures produced by RNAfold. Histogram showing the distribution of these performance metric across all structures in all sequences is shown in Figure 5. As we can see from the figure, majority of the RNAfold-generated structures can be recovered with larger than 0.8 sensitivity and PPV.

#### 3.2 Structure with pseudoknot

Although trained on synthetic dataset with no pseudoknot structures, since our model doesn't incorporate hard-wired rules on how local structures assemble into global structure, it is actually capable of generating structure with pseudoknots. As an example, we use the sequence of mouse mammary tumor virus (MMTV), whose secondary structure contains pseudoknot as measure by nuclear magnetic resonance (NMR), as shown in Fig 6(a). Minimum free energy structure predicted by RNAfold takes a quite different form, which is shown in Fig 6(b). In contrast, when we sampled 100 structures from our model, we observed a diverse set of structures, including the one predicted by RNAfold, as shown in Fig 6(c3), and more interestingly, the pseudoknot structure from NMR, as shown in Fig 6(c1).

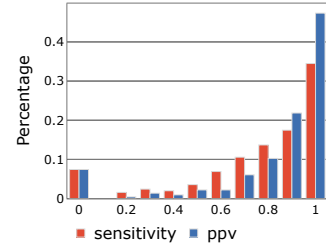


Figure 5: Performance on test set.

#### 3.3 Sequence design via gradient ascent

One benefit of having a differentiable model like neural network is that we can answer interesting questions like: given my current input sequence, what (small) changes can I make to maximize the pairing probability of two positions? We illustrate this using a short RNA sequence GAUCACCUU-UGGAUC. The sequence is short enough such that vast majority of the structures in the distribution are identical, as shown in Fig 7(a). In order to find small, local changes to be made on this sequence, given the current predicted structure, we computed the gradient of a selected output node with respect to all the input nodes  $\partial y_{i,j} / \partial x$ . We ran 100 gradient ascent iterations with step size 0.01, in each step, after adding the gradient (times step size) onto the input, we re-normalize the input so the feature dimension sum up to 1. After all 100 iterations, we convert the one-hot-encoding back to sequence by taking the nucleotide with max score for each position. Fig 7(b) and (c) shows the resulting sequence and structure for  $i = 5, j = 11$  and  $i = 6, j = 10$ , respectively.

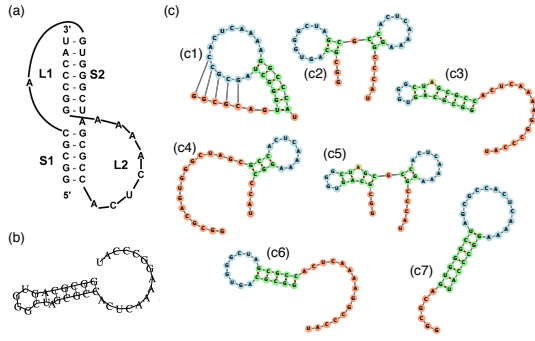


Figure 6: Secondary structure of mouse mammary tumor virus (MMTV): (a) measured by nuclear magnetic resonance (NMR), plot from [11], (b) predicted by RNAfold, (c) Structures generated by our model.

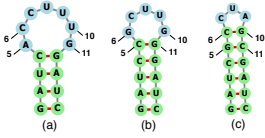


Figure 7: Gradient ascent to maximize base pairing. (a) position (5, 11), (b) position (6, 10).

## References

- [1] Ronny Lorenz, Stephan H Bernhart, Christian Höner Zu Siederdissen, Hakim Tafer, Christoph Flamm, Peter F Stadler, and Ivo L Hofacker. Viennarna package 2.0. *Algorithms for molecular biology*, 6(1):26, 2011.
- [2] Michael Zuker. Mfold web server for nucleic acid folding and hybridization prediction. *Nucleic acids research*, 31(13):3406–3415, 2003.
- [3] Mirela Andronescu, Anne Condon, Holger H Hoos, David H Mathews, and Kevin P Murphy. Efficient parameter estimation for rna secondary structure prediction. *Bioinformatics*, 23(13):i19–i28, 2007.
- [4] Stefanie A Mortimer, Mary Anne Kidwell, and Jennifer A Doudna. Insights into rna structure and function from genome-wide studies. *Nature reviews Genetics*, 15(7):469, 2014.
- [5] Philip C Bevilacqua, Laura E Ritchey, Zhao Su, and Sarah M Assmann. Genome-wide analysis of rna secondary structure. *Annual review of genetics*, 50:235–266, 2016.
- [6] Peter Kerpedjiev, Stefan Hammer, and Ivo L Hofacker. Forna (force-directed rna): simple and effective online rna secondary structure diagrams. *Bioinformatics*, 31(20):3377–3379, 2015.
- [7] Michelle J Wu. Convolutional models of rna energetics. *bioRxiv*, page 470740, 2018.
- [8] Devin Willmott, David Murrugarra, and Qiang Ye. State inference of rna secondary structures with deep recurrent neural networks.
- [9] Hao Zhang, Chunhe Zhang, Zhi Li, Cong Li, Xu Wei, Borui Zhang, and Yuanning Liu. A new method of rna secondary structure prediction based on convolutional neural network and dynamic programming. *Frontiers in genetics*, 10, 2019.
- [10] Linyu Wang, Yuanning Liu, Xiaodan Zhong, Haiming Liu, Chao Lu, Cong Li, and Hao Zhang. Dmfold: A novel method to predict rna secondary structure with pseudoknots based on deep learning and improved base pair maximization principle. *Frontiers in genetics*, 10:143, 2019.
- [11] David W Staple and Samuel E Butcher. Pseudoknots: Rna structures with diverse functions. *PLoS biology*, 3(6):e213, 2005.